Shock and Vibration 20 (2013) 273–286
DOI 10.3233/SAV-2012-00743
IOS Press

Effects of eccentricity on the dynamic behavior for electromechanical integrated toroidal drive

Lizhong Xu* and Haifeng Li
Mechanical Engineering Institute, Yanshan University, Qinhuangdao, Hebei, China

Received 21 December 2011
Revised 1 September 2012
Accepted 9 September 2012

Abstract. In electromechanical integrated toroidal drive, eccentric center errors occur which has important influences on the dynamic behavior of the drive system. Here, the dynamic equations of the drive system with eccentric center are presented. Changes of the natural frequencies and vibrating modes along with eccentric center distance are analyzed. The forced responses of the drive system to eccentric center excitation are investigated. Results show that the eccentric center causes some natural frequencies to increase, and the other natural frequencies to drop. It also causes some vibrations to become weak, and the other vibrations to become strong. The eccentric center has more obvious effects on the dynamic behavior of the planets. The results are useful in design and manufacture of the drive systems.

Keywords: Toroidal drive, electromechanical integrated, dynamic behavior, eccentricity

1. Introduction

As more and more electrical and control techniques are utilized in mechanical engineering field, electromechanical integrated drive systems are finding more applications in advanced mechanical science. In 1963, an electromechanical integrated electromagnetic harmonic drive was proposed by Herdeg [1]. In the drive system, the meshing forces between flexible gear and rigid gear are controlled by electromagnetic force, and drive, power and control are integrated. It has been used in the fields such as submarine navigation, etc, that require compactness [2]. In 2000, Oliver Barth proposed piezoelectric harmonic drive [3]. Here, the size of the electromechanical system was further decreased. In 2006, Lizhong Xu proposed an electrostatic harmonic drive in which the harmonic drive principle is used first in MEMS fields [4,5]. The magnetic gear drive is another type of the integrated drive system. In 1991, the magnetic gear drive was proposed and the torque test was done [6]. In 2006, a new cycloid permanent magnetic gear drive was proposed [7]. The main advantage of the permanent magnet gearing is meshing without contact.

Toroidal drive can transmit a large torque in a very small size and is suitable for technical applications such as aviation and space flight [8,10]. Based on research on toroidal drive [11], the authors have presented a novel integrated drive system, an electromechanical integrated toroidal drive. In the drive system, power and control are integrated. Compared with the toroidal drive, the new drive is easy to produce. It is without wear and does not need lubrication. Besides the above-mentioned fields that require compactness, the drive can be used with robots and in other fields that require accurate control.

*Corresponding author: Lizhong Xu, Mechanical Engineering Institute, Yanshan University, Qinhuangdao 066004, Hebei, China. Tel.: +86 335 8060195; Fax: +86 335 8074783; E-mail: xlz@ysu.edu.cn.

ISSN 1070-9622/13/$27.50

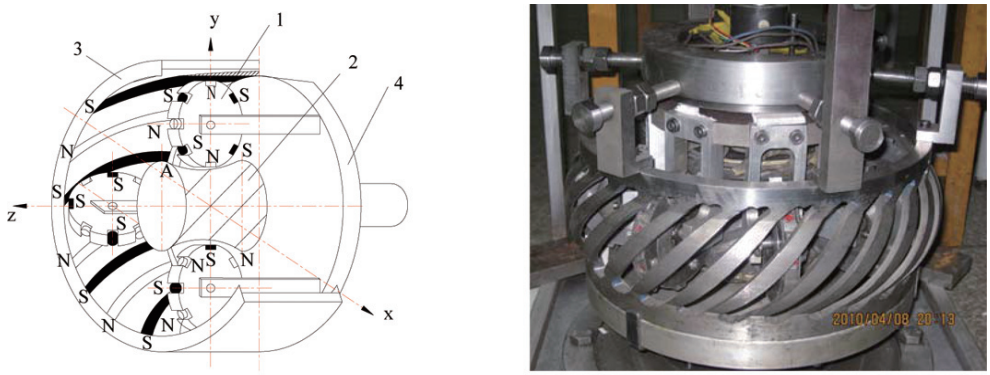

(a) drive structure (b) model machine

Fig. 1. Electromechanical integrated toroidal drive. 1. planet; 2. worm; 3. stator; 4. rotor.

The drive consists of four basic parts as shown in Fig. 1: (a) radically positioned planets; (b) the central worm; (c) a toroidal shaped stator; and (d) a rotor, which forms the central output shaft upon which the planets are mounted. The central worm is fixed and coils are mounted in helical grooves of its surface. The planets have permanent magnets instead of teeth. The N and S polar permanent magnets are mounted alternately on a planet. The stator has helical permanent magnets instead of helical teeth. In the same manner as planet, the N and S polar helical permanent magnets are mounted alternately on the stator.

For the electromechanical integrated toroidal drive, the forces, dynamics and the control theory of the drive system were investigated. In 2005, a dynamic model of the electromechanical integrated toroidal drive was established, and the natural frequencies and the vibrating modes of the drive system were analyzed [12]. In 2006, a control model of the drive system was proposed and the torque control of the drive system was investigated [13]. In 2010, forces and stress of the drive system were analyzed, and the force and stress distribution in the stator was determined [14]. However, process and mounting errors exist in the drive system. The eccentric center is a main form of the errors which has important influences on the dynamic behavior of the drive system. The effects of the eccentric center on the dynamic behavior of the drive system have not been studied yet.

In this paper, the electromagnetic mesh stiffness equations of the drive system with eccentric center are deduced. Based on them, the dynamic equations for the drive system with eccentric center are given. Using these equations, changes of the natural frequencies and vibrating modes along with eccentric center distance are analyzed, and the forced responses of the drive system to eccentric center excitation are investigated. Results show that vibration modes of the drive system can be classified into rotational mode, planet mode and special planet mode. For rotational mode and planet mode, the eccentric center causes some natural frequencies to increase, and the other natural frequencies to drop. For special planet mode, the eccentric center has not effects on the natural frequencies. For rotational mode and the planet mode, the eccentric center causes some vibrations to become weak, and the other vibrations to become strong. The results are useful in design and manufacture of the drive systems.

2. Electromagnetic mesh stiffness with eccentric center

Space phase relation of the worm coils is shown in Fig. 2. The symbol ϕ_v denotes the face width angle of the worm. Then, in the transverse plane of the planet, the phase angle of the phase-i is

$$\phi_i = \frac{i-1}{n}\frac{\phi_v}{p} \quad (i = 1 \text{ to } n) \tag{1}$$

where n is the phase number of the worm coils ($n = 3$) and p is the number of the pole-pairs.

Let the position angle $\theta = 0$ of the planet when tooth of the planet is aligned completely with phase-A coil. Inductances of the every phase can be calculated as follows

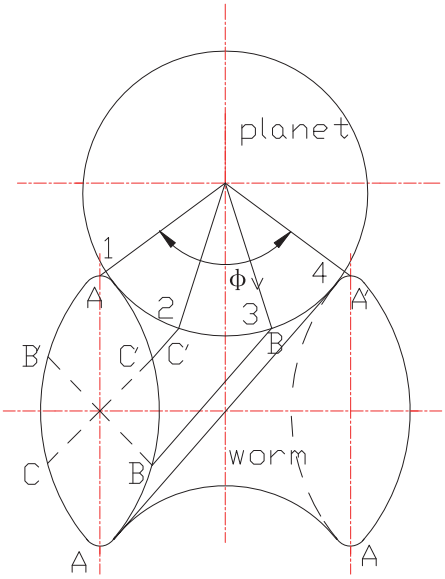

Fig. 2. Space phase relation of the worm coils.

Self-inductances:

$$L_{ii} = L_0 + L_1 \cos\left(z_1\theta - (i-1)\frac{\phi_v}{pn}\right) (i = 1 \text{ to } n) \tag{2-a}$$

Mutual-inductances between adjacent phases:

$$L_{i-1,i} = L_{01} + L_1 \cos\left(z_1\theta - (2i-3)\frac{\phi_v}{2pn}\right) (i = 2 \text{ to } n) \tag{2-b}$$

Mutual-inductances between two spacing phases:

$$L_{i-2,i} = L_{02} + L_1 \cos\left(z_1\theta - (2i-4)\frac{\phi_v}{2pn}\right) (i = 3 \text{ to } n) \tag{2-c}$$

where $L_{0i} = L_0 \cos\frac{i\phi_v}{pn}$ ($i = 1$ to n), L_0 is the average inductance, L_1 is the first harmonic component of the inductance, z_1 is the tooth number of the planet.

The magnetic linkage λ_{is} of the central worm coils is $\lambda_{is} = \sum_{j=1}^{n} L_{ij} I_{is}$ and the magnetic energy storage between a tooth of the planet and worm is $W = \sum_{j=1}^{n}\sum_{i=1}^{n} L_{ij} I_{is} I_{js}$. Thus, the electromechanical coupled force between a tooth of the planet and worm is given as

$$F_{wpi} = -\frac{1}{(R + e_{wpi})}\frac{\partial W}{\partial \theta} = -\frac{1}{2(R + e_{wpi})}\sum_{j=1}^{n}\sum_{i=1}^{n}\frac{dL_{ij}}{d\theta} I_{is} I_{js} \tag{3}$$

where L_{ij} is the inductances of the every phase, I_{is} is the current of the ith phase worm coils, here e_{wpi} is the eccentric center distance between the planet i and the worm, R is the calculative radius of the planet.

Equation (3) can be simplified as

$$F_{wpi} = k_{wpi}\zeta_{wpi} \tag{4}$$

where ζ_{wpi} is the relative displacement between planet and worm, $\zeta_{wpi} = (R + e_{wpi})\delta\theta$, k_{wpi} is considered as electromagnetic mesh stiffness between a tooth of the planet and worm,

$$k_{wpi} = -\frac{1}{2(R+e_{wpi})^2}\sum_{i=1}^{n}\sum_{i=1}^{n}\left(\frac{\delta^2 L_{ij}}{\delta\theta^2}\right) I_i I_j.$$

The electromagnetic mesh stiffness k_{spi} between a planet tooth and stator can be obtained in the same manner as k_{wpi}. Since the stator has the helical permanent magnets instead of helical teeth, the equivalent current I_{s0} of the permanent magnet teeth is constant. The electromechanical coupled force between a tooth of the planet and stator is given as

$$F_{spi} = k_{spi}\zeta_{spi} \tag{5}$$

where

$$k_{spi} = -\frac{1}{2(R+e_{spi})^2}\sum_{i=1}^{n}\sum_{i=1}^{n}\left(\frac{\delta^2 L_{ij}}{\delta\theta^2}\right) I_{s0}^2,$$

it is considered as electromagnetic mesh stiffness between a tooth of the planet and the stator, here e_{spi} is the eccentric center distance between the planet i and the stator.

3. The dynamic equations of the drive system with eccentric center

Figure 3 gives the dynamic model of a toroidal drive with eccentric center. The toroidal drive in Fig. 3(a) is considered as a combination of three sub-systems (i) a worm/planet pair [Fig. 3(b)], (ii) a stator/planet pair [Fig. 3(c)], and (iii) a rotor/planet pair [Fig. 3(d)]. The eccentric center consists of the average eccentric center and the dynamic eccentric center. The average eccentric center changes the electromagnetic meshing stiffness, and the dynamic eccentric center becomes the dynamic excitation to the drive system.

The dynamic model allows stator, rotor and each planet to rotate about these translational axes. For the sake of convenience, the rotations are replaced by their corresponding translational displacements as

$$u_j = r_j\theta_j,\ (j = w, s, p, r)$$

where θ_j is the rotation of worm, stator, rotor and planet, r_j is the rolling circle radius for worm, stator and planet, and the radius of the circle passing through planet centers for the rotor.

Figure 3(b) shows a worm/planet pair which represents the worm (subscript w) meshing with planet-i (subscript pi). Here, γ_{wpi} is the lead angle of the helix tooth at reference circle on the worm and λ is the equivalent tooth shape angle of the planet tooth; k_{wp} is the mesh stiffness between the planet and the worm. The model allows planets to rotate about their own axes. It also allows planets to translate in x and y directions. The symbols x_{pi} and y_{pi} denote the displacements of the planet in x and y directions, respectively.

From the balance conditions of the worm and the planet, ones can give

$$\begin{cases} m_{pi}\ddot{u}_i + c_{wpi}\dot{v}_{wpi}\sin\gamma_{wpi} - k_{wpi}\left(p_{wpi} + e_{wpi}\sin\lambda\right)\sin\gamma_{wpi}\cos\lambda = 0 \\ m_i\ddot{x}_i + k_{wpi}\left(p_{wpi} + e_{wpi}\sin\lambda\right)\sin\lambda = 0 \\ m_i\ddot{z}_i + c_{wpi}\dot{v}_{wpi}\cos\gamma_{wpi} - k_{wpi}\left(p_{wpi} + e_{wpi}\sin\lambda\right)\cos\gamma_{wpi}\cos\lambda = 0 \end{cases} \tag{6}$$

where m_i and m_{pi} are the mass and equivalent mass of the planet, respectively, $m_{pi} = J_{pi}/r_p^2$; M_w is the equivalent mass of the worm, $M_w = J_w/r_w^2$; J_{pi} and J_w are the polar mass moments of inertia for the planet and worm, respectively; p_{wpi} is the relative displacement between the planet-i and the worm, $p_{wpi} = -u_i\sin\gamma_{wpi}\cos\lambda + x_i\sin\lambda - z_i\cos\gamma_{wpi}\cos\lambda$ and $v_{wpi} = -u_i\sin\gamma_{wpi} - z_i\cos\gamma_{wpi}$.

Substituting p_{wpi} and v_{wpi} into Eq. (6), the dynamic equations in matrix form can be given

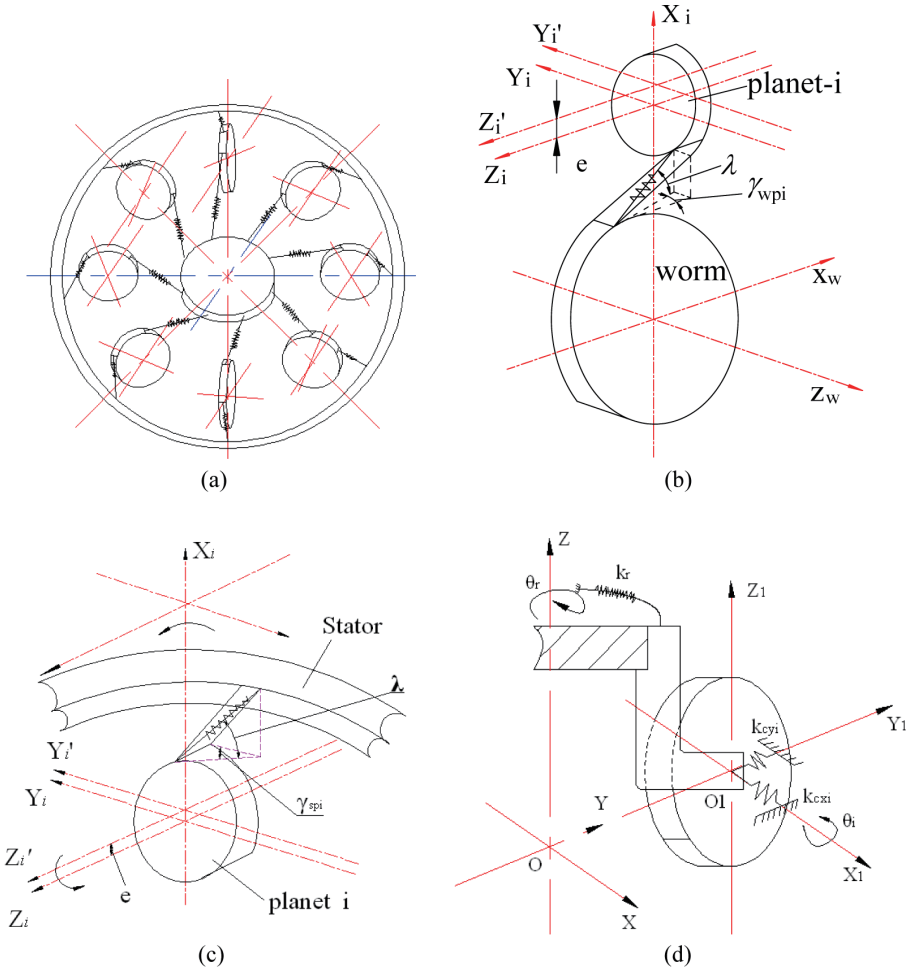

Fig. 3. Dynamic models of (a) a eight-planet toroidal drive, (b) a worm/planet pair, (c) a stator/planet pair, and (d) a rotor/planet pair.

$$\boldsymbol{m}_i\ddot{\boldsymbol{q}}_i + \boldsymbol{c_{wpi}}\boldsymbol{q_i} + \boldsymbol{k_{wpi}}\boldsymbol{q_i} = \boldsymbol{F_{wpi}} \tag{7}$$

where $\boldsymbol{q}_i = [u_i, x_i, z_i]^T$, it is the displacement vector of the planet; $\boldsymbol{m}_{ii} = Diag[m_{pi}, m_i, m_i]$, it is the mass matrix of the planet;

$$\boldsymbol{k_{wpi}} = k_{wpi}\begin{bmatrix} \sin^2\gamma_{wpi}\cos^2\lambda & -\sin\gamma_{wpi}\sin\lambda\cos\lambda & \sin\gamma_{wpi}\cos\gamma_{wpi}\cos^2\lambda \\ -\sin\gamma_{wpi}\sin\lambda\cos\lambda & \sin^2\lambda & -\cos\gamma_{wpi}\sin\lambda\cos\lambda \\ \sin\gamma_{wpi}\cos\gamma_{wpi}\cos^2\lambda & -\cos\gamma_{wpi}\sin\lambda\cos\lambda & \cos^2\gamma_{wpi}\cos^2\lambda \end{bmatrix}$$

$$\boldsymbol{F_{wpi}} = k_{wpi}\begin{bmatrix} e_{wpi}\sin\gamma_{wpi}\sin\lambda\cos\lambda \\ -e_{wpi}\sin^2\lambda \\ e_{wpi}\cos\gamma_{wpi}\sin\lambda\cos\lambda \end{bmatrix}$$

$$\boldsymbol{c_{wpi}} = c_{wpi}\begin{bmatrix} -\sin^2\gamma_{wpi} & 0 & -\cos\gamma_{wpi}\sin\gamma_{wpi} \\ 0 & 0 & 0 \\ -\cos\gamma_{wpi}\sin\gamma_{wpi} & 0 & -\cos^2\gamma_{wpi} \end{bmatrix}$$

Figure 3(c) illustrates a stator/planet pair which represents the stator (subscript$s$) meshing with planet-i. Here, γ_{spi} is the lead angle of the helix tooth at reference circle on the stator; k_{sp} is the mesh stiffness between the planet and the stator.

The model allows stator and planet to rotate about their own axes. It also allows planet to translate in$x$ and $y$directions. From force and torque balance conditions of the stator and the planet, ones can give

$$\begin{cases} M_s\ddot{u}_s - k_{spi}\left(p_{spi} - e_{spi}\sin\lambda\right)\cos\lambda\sin\gamma_{spi} = 0 \\ m_{pi}\ddot{u}_i + c_{spi}\dot{v}_{spi}\cos\gamma_{spi} + k_{spi}\left(p_{spi} - e_{spi}\sin\lambda\right)\cos\lambda\cos\gamma_{spi} = 0 \\ m_i\ddot{x}_i - k_{spi}\left(p_{spi} - e_{spi}\sin\lambda\right)\sin\lambda = 0 \\ m_i\ddot{z}_i + c_{spi}\dot{v}_{spi}\sin\gamma_{spi} + k_{spi}\left(p_{spi} - e_{spi}\sin\lambda\right)\cos\lambda\sin\gamma_{spi} = 0 \end{cases} \tag{8}$$

where M_s is the equivalent mass of the stator, $M_s = J_s/r_s^2$, J_s is the polar mass moments of inertia for the stator; p_{spi} is the relative displacement between the stator and the planet, $v_{spi} = u_i\cos\gamma_{spi} + z_i\sin\gamma_{spi}$ and $p_{spi} = -u_s\sin\gamma_{spi}\cos\lambda + u_i\cos\gamma_{spi}\cos\lambda - x_i\sin\lambda + z_i\sin\gamma_{spi}\cos\lambda$.

Substituting p_{spi} and v_{spi} into Eq. (8), the dynamic equations in matrix form can be given

$$\begin{bmatrix} M_s & \mathbf{0} \\ \mathbf{0} & \boldsymbol{m}_i \end{bmatrix}\begin{bmatrix} \ddot{u}_s \\ \ddot{\boldsymbol{q}}_i \end{bmatrix} + \begin{bmatrix} 0 & 0 \\ 0 & \boldsymbol{c_{spi}} \end{bmatrix}\begin{bmatrix} \dot{u}_s \\ \dot{\boldsymbol{q}}_i \end{bmatrix} + \begin{bmatrix} k_{usi} & \boldsymbol{k}_{si}^T \\ \boldsymbol{k}_{si} & \boldsymbol{k}_{spi} \end{bmatrix}\begin{bmatrix} u_s \\ \boldsymbol{q}_i \end{bmatrix} = \begin{bmatrix} F_{si} \\ \boldsymbol{F_{spi}} \end{bmatrix} \tag{9}$$

where $k_{usi} = k_{spi}\sin^2\gamma_{spi}\cos^2\lambda$

$$\boldsymbol{k}_{si}^T = k_{spi}\begin{bmatrix} -\sin\gamma_{spi}\cos\gamma_{spi}\cos^2\lambda & \sin\gamma_{spi}\sin\lambda\cos\lambda & -\sin^2\gamma_{spi}\cos^2\lambda \end{bmatrix}$$

$$\boldsymbol{k_{spi}} = k_{spi}\begin{bmatrix} \cos^2\gamma_{spi}\cos^2\lambda & -\cos\gamma_{spi}\sin\lambda\cos\lambda & \sin\gamma_{spi}\cos\gamma_{spi}\cos^2\lambda \\ -\cos\gamma_{spi}\sin\lambda\cos\lambda & \sin^2\lambda & -\sin\gamma_{spi}\sin\lambda\cos\lambda \\ \sin\gamma_{spi}\cos\gamma_{spi}\cos^2\lambda & -\sin\gamma_{spi}\sin\lambda\cos\lambda & \sin^2\gamma_{spi}\cos^2\lambda \end{bmatrix}$$

$$F_{si} = -k_{spi}e_{spi}\sin\gamma_{spi}\sin\lambda\cos\lambda$$

$$\boldsymbol{F_{spi}} = \begin{bmatrix} k_{spi}e_{spi}\cos\gamma_{spi}\sin\lambda\cos\lambda \\ -k_{spi}e_{spi}\sin^2\lambda \\ k_{spi}e_{spi}\sin\gamma_{spi}\sin\lambda\cos\lambda \end{bmatrix}$$

$$\boldsymbol{c_{spi}} = c_{spi}\begin{bmatrix} \cos^2\gamma_{spi} & 0 & \sin\gamma_{spi}\cos\gamma_{spi} \\ 0 & 0 & 0 \\ \sin\gamma_{spi}\cos\gamma_{spi} & 0 & \sin^2\gamma_{spi} \end{bmatrix}$$

Figure 3(d) shows the model of the rotor/planet pair. From the balance conditions of the rotor and the planet, ones can give

$$\begin{cases} m_{pi}\ddot{u}_i = 0 \\ m_i\ddot{x}_i + c_{cpxi}\dot{x}_i + k_{cpxi}x_i = 0 \\ m_i\ddot{z}_i + c_{cpxi}\dot{z}_i + k_{cpzi}z_i = 0 \end{cases} \tag{10}$$

Equation (10) can be given in matrix form as

$$\boldsymbol{m}_i\ddot{\boldsymbol{q}}_i + \boldsymbol{c_{cpi}}\dot{\boldsymbol{q}}_i + \boldsymbol{k}_{cpi}\boldsymbol{q}_i = 0 \tag{11}$$

where

$$\boldsymbol{k}_{cpi} = \begin{bmatrix} 0 & 0 & 0 \\ 0 & k_{cxi} & 0 \\ 0 & 0 & k_{czi} \end{bmatrix}$$

$$\boldsymbol{c}_{cpi} = \begin{bmatrix} 0 & 0 & 0 \\ 0 & c_{cpxi} & 0 \\ 0 & 0 & c_{cpzi} \end{bmatrix}$$

Equations (7), (9) and (11) can be combined systematically to obtain the dynamics equations of the overall toroidal drive which consists of a worm, a stator, a rotor and m planets ($i = 1$ to m). The dynamic model of the drive system is given in Fig. 3(a).

The dynamic equations of the $3m+1$ DOF model of the toroidal drive are given in matrix form as

$$\boldsymbol{M}\ddot{X} + \boldsymbol{C}\dot{X} + \boldsymbol{K}X = \boldsymbol{F} \tag{12}$$

where

$$\boldsymbol{X} = [\boldsymbol{q}_1 \ \cdots \ \cdots \ \boldsymbol{q}_m \ u_s]^T$$

$$\boldsymbol{M} = diag\,[\boldsymbol{m}_1 \ \cdots \ \cdots \ \boldsymbol{m}_m \ M_s]$$

$$\boldsymbol{K} = \begin{bmatrix} \boldsymbol{k}_{11} & \cdots & \cdots & \boldsymbol{0} & \cdots & \cdots & \boldsymbol{0} & \boldsymbol{k}_{s1} \\ & \cdots & \cdots & & & & & \cdots \\ & & \cdots & & & & & \cdots \\ & & & \boldsymbol{k}_{ii} & & & & \boldsymbol{k}_{si} \\ & & & & \cdots & & & \cdots \\ & symmetric & & & & \cdots & & \cdots \\ & & & & & & \boldsymbol{k}_{mm} & \boldsymbol{k}_{sm} \\ & & & & & & & \sum_{i=1}^{m} k_{usi} \end{bmatrix}$$

$$\boldsymbol{k}_{ii} = \boldsymbol{k}_{wpi} + \boldsymbol{k}_{spi} + \boldsymbol{k}_{cpi}$$

$$\boldsymbol{C} = \begin{bmatrix} \boldsymbol{c}_{11} & \cdots & \cdots & \boldsymbol{0} & \cdots & \cdots & \boldsymbol{0} & 0 \\ & \cdots & \cdots & & & & & \cdots \\ & & \cdots & & & & & \cdots \\ & & \boldsymbol{c}_{ii} & & & & & 0 \\ & & & & \cdots & & & \cdots \\ & symmetric & & & & \cdots & & \cdots \\ & & & & & & \boldsymbol{c}_{mm} & 0 \\ & & & & & & & 0 \end{bmatrix}$$

$$\boldsymbol{c}_{ii} = \boldsymbol{c}_{wpi} + \boldsymbol{c}_{spi} + \boldsymbol{c}_{cpi}$$

$$\boldsymbol{F} = \left[\boldsymbol{F_{wp}}_1 + \boldsymbol{F_{sp}}_1 \cdots \boldsymbol{F_{wpi}} + \boldsymbol{F_{spi}} \cdots F_{si}\right]^T$$

4. The solution of the dynamic equations

The total eccentric center consists of the average eccentric center and the dynamic eccentric center ($e = \overline{e} + \Delta e$). Hence, the equivalent load vector of the eccentric center is

$$\boldsymbol{F} = \overline{\boldsymbol{F}} + \Delta\boldsymbol{F} \tag{13}$$

where $\overline{\boldsymbol{F}}$ is the average load vector dependent on the average eccentric center, $\Delta\boldsymbol{F}$ is the dynamic load vector dependent on the dynamic eccentric center.

Thus, the total displacement vector consists of the average displacement vector and the dynamic displacement vector

$$\boldsymbol{X} = \overline{\boldsymbol{X}} + \Delta\boldsymbol{X} \tag{14}$$

where $\overline{\boldsymbol{X}}$ is the average displacement vector and $\Delta\boldsymbol{X}$ is the dynamic displacement vector.

Substituting Eqs (13) and (14) into Eq. (12), and neglecting nonlinear terms, yields

$$\mathbf{K}\overline{\mathbf{X}} = \overline{\mathbf{F}} \tag{15}$$

$$\boldsymbol{M}\Delta\ddot{\boldsymbol{X}} + \boldsymbol{C}\Delta\boldsymbol{X} + \boldsymbol{K}\Delta\boldsymbol{X} = \Delta\boldsymbol{F} \tag{16}$$

Table 1
Parameters of the example system

γ_{wpi} (°)	γ_{spi} (°)	M_s (kg)	m_i (kg)	m_{pi} (kg)	k_{cxi} (N/m)	k_{czi} (N/m)	λ (°)
25	45	13	0.97	0.485	1.4×10^6	2.8×10^6	0

Table 2
Natural frequencies of the drive system with eccentric center worm (rad/s)

	$m = 2$			$m = 4$	
	$e = 0$	$e = 0.5$ *mm*		$e = 0$	$e = 0.5$ *mm*
$n = 1$	9.5045	9.5042	$n = 1$	13.1255	13.1253
	88.1570	88.1627		90.2644	90.2657
	284.1614	284.2683		284.2058	284.2785
$n = m - 1$	86.0449	86.0388	$n = m - 1$	86.0449	85.9611
					86.0449
					86.1271
	284.1175	284.0106		284.1175	284.0054
					284.1175
					284.1569
$n = m$	191.2046	191.2046	$n = m$	191.2046	191.2046

The homogeneous part of Eq. (12) is used for the free vibration analysis of the drive system. The governing eigenvalue problem yields natural frequencies and corresponding vibrating modes. The average displacement vector $\overline{\boldsymbol{X}}$ is obtained from Eq. (15). The dynamic response of the drive system to dynamic eccentric center can be obtained from Eq. (16).

Equation (16) can be transmitted into regular equation as below

$$\boldsymbol{M}_N\ddot{\boldsymbol{q}}_N + \boldsymbol{C}_N\dot{\boldsymbol{q}}_N + \boldsymbol{K}_N\boldsymbol{q}_N = \boldsymbol{F}_N \tag{17}$$

where $\boldsymbol{M}_N$, $\boldsymbol{C}_N$ and $\boldsymbol{K}_N$ are the diagonal mass, damping and mean stiffness matrices, respectively. $\boldsymbol{F}_N$ and $\boldsymbol{q}_N$ are the transmitted equivalent exciting force and displacement vectors, respectively. They can be calculated as

$$\boldsymbol{M}_N = \boldsymbol{A}_N^T\boldsymbol{M}\boldsymbol{A}_N, \quad \mathrm{K}_N = \boldsymbol{A}_N^T\boldsymbol{K}\boldsymbol{A}_N, \quad \boldsymbol{C}_N = \boldsymbol{A}_N^T\boldsymbol{C}\boldsymbol{A}_N, \boldsymbol{q}_N = \boldsymbol{A}_N^T\Delta\boldsymbol{X} \text{ and } \boldsymbol{F}_N = \boldsymbol{A}_N^T\Delta\boldsymbol{F}$$

Here, $\boldsymbol{A}_N$ is the mode matrix of the Eq. (12).

Since the equivalent exciting forces change periodically, the solution of each equation in Eq. (17) can be obtained as below

$$q_{Nr} = \frac{1}{m_r\omega_{dr}}\int_0^t F_{Nr}(\tau)e^{-\xi\omega_{nr}(t-\tau)}\sin\omega_{dr}(t-\tau)d\tau \tag{18}$$

where ω_{dr} is the natural frequency of the drive system ($r = 1$ to $3m+1$), $\omega_{dr} = \omega_{nr}\sqrt{1-\xi_r^2}$, ξ_r is the damping coefficient; m_r is the transmitted mass, $F_{Nr}(\tau)$ is the equivalent exciting force.

Substituting $F_{Nr}(\tau) = E_r\sin\omega_e t$ into Eq. (18), yields

$$\begin{aligned} q_{Nr} \;=\; & \frac{E_r}{\omega_{dr}}\left\{\frac{e^{-\xi_r\omega_{nr}t}\left[\xi_r\omega_{nr}\cos\omega_{dr}t - (\omega_{dr}-\omega_e)\sin\omega_{dr}t\right] - \xi_r\omega_{nr}\cos\omega_e t + (\omega_{dr}-\omega_e)\sin\omega_e t}{(\omega_{dr}-\omega_e)^2 + (\xi\omega_{nr})^2}\right. \\ & \left. + \frac{e^{-\xi_r\omega_{nr}t}\left[(\omega_{dr}+\omega_e)\sin\omega_{dr}t - \xi_r\omega_{nr}\cos\omega_{dr}t\right] + \xi_r\omega_{nr}\cos\omega_e t + (\omega_{dr}+\omega_e)\sin\omega_e t}{(\omega_{dr}+\omega_e)^2 + (\xi\omega_{nr})^2}\right\} \end{aligned} \tag{19}$$

where ω_e is the exciting frequency of the dynamic eccentric center, E_r is the amplitude of the equivalent exciting force.

From q_{Nr}, the real dynamic displacements $\Delta\boldsymbol{X}$ of the drive system can be obtained

$$\Delta\boldsymbol{X} = \boldsymbol{A}_N\boldsymbol{q}_N \tag{20}$$

Table 3(a)
Modes of the drive system without eccentric center

ω_i(rad/s)	9.5045	88.1570	284.1614	86.0449	284.1175	191.2046
u_i	−0.8236	−1	−0.1371	1	0.1365	0
x_i	0	0	0	0	0	1
z_i	0.0106	0.0714	−1	−0.0683	1	0
u_i	−0.8236	−1	−0.1371	−1	−0.1365	0
x_i	0	0	0	0	0	0
z_i	0.0106	0.0714	−1	0.0683	−1	0
u_s	−1	0.0616	0.0068	0	0	0

Table 3(b)
Modes of the drive system with eccentric center worm

ω_i(rad/s)	9.5042	88.1627	284.2683	86.0388	284.0106	191.2046
u_i	−0.8210	−1	−0.1376	0.9019	0.0115	0
x_i	0	0	0	0	0	1
z_i	0.0107	0.0716	−1	−0.0617	0.0860	0
u_i	−0.8263	−0.8970	−0.0120	−1	−0.1360	0
x_i	0	0	0	0	0	0
z_i	0.0104	0.0638	−0.0858	0.0680	−1	0
u_s	1	0.0584	0.0037	0.0032	0.0031	0

Table 4
Natural frequencies of the drive system with eccentric center stator (rad/s)

$m = 2$			$m = 4$		
	$e = 0$	$e = 0.5$ mm		$e = 0$	$e = 0.5$ mm
$n = 1$	9.5045	9.5043	$n = 1$	13.1255	13.1254
	88.1570	88.2825		90.2644	90.2986
	284.1614	284.2599		284.2058	284.2712
$n = m - 1$	86.0449	85.9151	$n = m - 1$	86.0449	85.6575
					86.0449
					86.3938
	284.1175	284.0192		284.1175	284.0139
					284.1175
					284.1559
$n = m$	191.2046	191.2046	$n = m$	191.2046	191.2046

5. Results and discussion

The above related equations are utilized for analysis of the free vibration for the drive system with eccentric center. The parameters of the example drive system are shown in Table 1. Table 2 gives the natural frequencies of the drive system with eccentric center worm. Here, the drive systems with two and four planets are considered. Table 3 shows the vibrating modes of the drive system with and without eccentric center. Table 4 gives the natural frequencies of the drive system with eccentric center stator. Table 5 gives the natural frequencies of the drive system with eccentric center planet. Tables 2–5 show:

(1) Three natural frequencies always have multiplicity $n = 1$ for different planet number m. Their values increase as additional planets are introduced. Their associated vibration modes have rotation of the stator, so these modes are named rotational modes. In a rotational mode, all planets have the same motion and move in phase (see the first-third columns in Table 3(a)). As the eccentric center of the worm occurs, three natural frequencies change slightly and the motions of the planets becomes different from each other (see the first-third columns in Table 3(b)). It is because the electromagnetic mesh stiffness between the worm and each planet becomes different from each other. Besides it, the vibration of the stator becomes weak, and some planet vibration becomes weak and the other planet vibration becomes strong when the eccentric center of the worm occurs. Here, $n = m - 1$, it is the multiplicity of the natural frequencies. For $m = 2$, $n = m - 1 = 1$. It means that each natural frequency only corresponds to one vibration mode. For $m = 3$, $n = m - 1 = 2$. It means that each natural frequency corresponds to two vibration modes.

Table 5
Natural frequencies of the drive system with eccentric center planet (rad/s)

	$m=2$				$m=4$		
	$e=0$	$e=0.5$ mm	$e=-0.5$ mm		$e=0$	$e=0.5$mm	$e=-0.5$mm
$n=1$	9.5045	9.5307	9.4773	$n=1$	13.1255	13.1445	13.1059
	88.1570	87.9575	88.3971		90.2644	90.1538	90.3915
	284.1614	284.1658	284.1579		284.2058	284.2076	284.2044
$n=m-1$	86.0449	85.8208	86.2261	$n=m-1$	86.0449	85.7323	86.3387
						86.0449	86.0449
						86.0449	86.0449
	284.1175	284. 1217	284.1124		284.1175	284.1243	284.1104
						284.1175	284.1175
						284.1175	284.1175
$n=m$	191.2046	191.2046	191.2046	$n=m$	191.2046	191.2046	191.2046

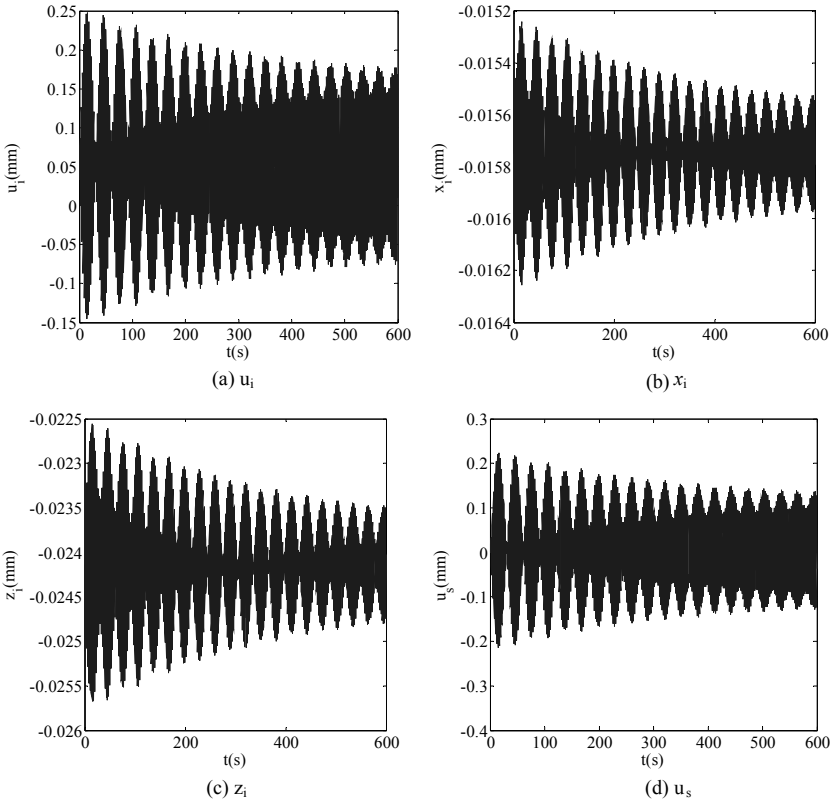

Fig. 4. The forced responses of the drive system to the dynamic eccentric center ($\omega = 81$ rad/s).

(2) Without the eccentric center, three natural frequencies have multiplicity $n = m-1$. These natural frequencies are independent of the numbers of planets. Their associated vibration modes are named planet modes because the stator does not move. Only planet motion occurs in these modes (see the fourth-fifth columns in Table 3(a)). As the eccentric center of the worm occurs, the multiplicity $n = m-1$ of three natural frequencies vanishes, and the planet's deflection relationship ($\boldsymbol{p}_i = w_i \boldsymbol{p}_1$) also does not exist(see the fourth-fifth columns in Table 3(b)). Three different natural frequencies occur, but the difference between them is relatively small. Besides it, the vibration of the stator occurs.

(3) One natural frequency always has multiplicity $n = m$ for different m. The natural frequency is independent of the numbers of planets. Its associated vibration modes are named special planet modes. For each of these modes, only one planet moves in transverse direction (see the sixth column in Tables 3(a) and (b)). The

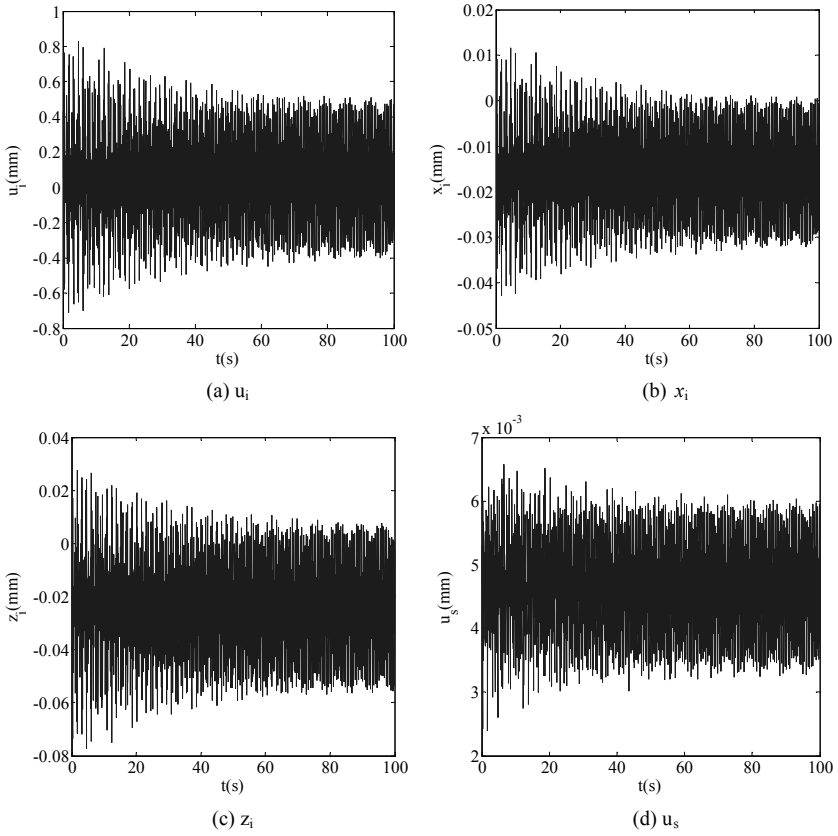

Fig. 5. The forced responses of the drive system to the dynamic eccentric center ($\omega = 540$ rad/s).

numbers of the single modes equal ones of the planets. As the eccentric center of the worm occurs, the natural frequency and the planet's deflection are not influenced.

(4) As the eccentric center of the stator occurs, three natural frequencies for the rotational modes change. For the planet modes, the multiplicity $n = m - 1$ of three natural frequencies vanishes, and three different natural frequencies occur. For the special planet modes, the natural frequencies are not influenced (see Table 4).

(5) As the eccentric center of the planet occurs, three natural frequencies for the rotational modes change: the positive eccentric center causes some natural frequencies to increase, and other natural frequencies to decrease; the effects of the negative eccentric center on the natural frequencies are opposite to ones of the positive eccentric center. Besides it, the vibration of the stator becomes weak.

For the planet modes, the multiplicity of the natural frequencies becomes $n = m - 2$, and one different natural frequency occurs. Besides it, the vibration of the stator occurs. For the special planet modes, the natural frequencies are still not influenced (see Table 5, here corresponding modes are not given).

The forced responses of the drive system to the dynamic eccentric center are investigated (see Figs 4–7). The parameters of the example system are given in Table 1 (here, $c_{wpi} = 0.1$ Ns/m and $c_{spi} = 0.1$ Ns/m). From Figs 4–7, ones know:

(1) As the exciting frequency of the eccentric center is 81 rad/s, the amplitudes of the rotational vibrations u_i and u_s are large, and the amplitudes of the translational vibrations x_i and z_i are small (see Fig. 4). It is because the exciting frequency 81 rad/s is near to one natural frequency of the rotational modes for the drive system. Here, the rotational mode plays a main role in the forced responses of the drive system to the eccentric center excitation. The amplitudes of the rotational vibrations u_i and u_s are about 10 times of the amplitudes of the translational vibrations x_i and z_i. The large amplitude of the rotational vibration u_s is the typical

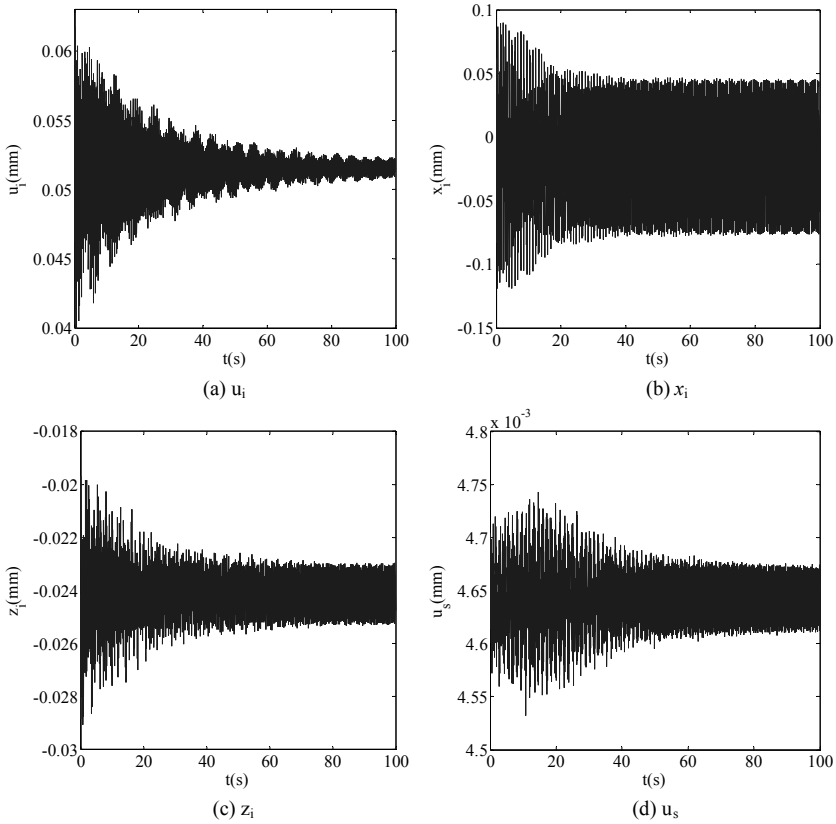

Fig. 6. The forced responses of the drive system to the dynamic eccentric center ($\omega = 1200$ rad/s).

characteristics of the rotational modes. Meanwhile, the vibration center shift of the drive system occurs which is caused by the average eccentric center. The vibration of the stator has more obvious effect on the dynamic behavior of the drive system. So, the eccentric center should be avoided and its exciting frequency should be far from the natural frequencies of the rotational modes.

(2) As the exciting frequency of the eccentric center is 540 rad/s, the amplitudes of the planet vibrations (u_i, x_i and z_i) are relatively large, and the amplitude of the stator vibration(u_s) is small (see Fig. 5). It is because the exciting frequency 540 rad/s is near to one natural frequency of the planet modes. Here, the planet mode plays a main role in the forced responses. Of course, the amplitude of the rotational vibration u_s is not zero. $u_s = 0$ is the typical characteristics of the planet modes. It is because the rotational mode plays a small role in the forced responses. Here, the amplitude of the rotational vibration u_i of the planet is the maximum (about 0.8 mm) which is larger than 100 times of the amplitude of the rotational vibration u_s of the stator. It will decrease operating stability of the drive system. Meanwhile, the vibration center shift of the drive system occurs as well. Here, the vibration center shift is identical to ones for the situation $\omega = 81$ rad/s. So, the exciting frequency of the eccentric center should be far from the natural frequencies of the planet modes as well.

(3) As the exciting frequency of the eccentric center is 1200 rad/s, the amplitude of the planet vibration (x_i) is relatively large, and the amplitudes of the stator vibration (u_s) and other vibrations (u_i and z_i) of the planet are small (see Fig. 6). It is because the exciting frequency 1200 rad/s is near to one natural frequency of the special planet modes. The maximum amplitude of the planet vibration (x_i) is about 0.1 mm, and the amplitudes of the other vibrations of the planet and the stator are not zero. It is because the special planet modes play a main role, and the other modes play a small role in the forced responses.

(4) As the exciting frequency of the eccentric center is 3000 rad/s, the vibrating amplitudes of the elements for the drive system are small (see Fig. 7). The amplitude of the rotational vibration u_i of the planet is the

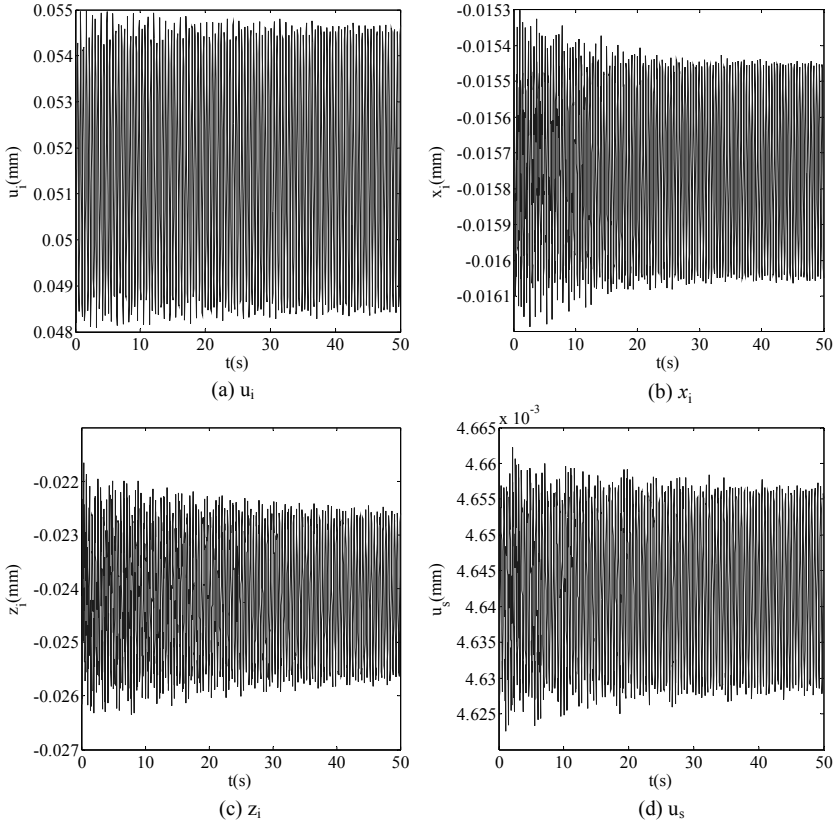

Fig. 7. The forced responses of the drive system to the dynamic eccentric center ($\omega = 3000$ rad/s).

maximum (about 3.5 μm). The amplitudes of the other vibrations x_i and z_i of the planet is the same orders of magnitude as the amplitude of the vibration u_i. The amplitude of the rotational vibration u_s is the smallest (about 0.02 μm). It is because the exciting frequency 3000 rad/s is far from the natural frequencies of the drive system.

In a word, the vibrations of the planet are the main vibrations of the drive system under the eccentric excitation. So, the dynamic design of the planets for the drive system should be considered first.

6. Conclusions

In this paper, the equations of the electromagnetic mesh stiffness for the electromechanical integrated toroidal drive with eccentric center are given. The dynamic equations for the drive system with eccentric center are deduced. Changes of the natural frequencies and vibration modes along with the eccentric center distance are analyzed, and the forced responses of the drive system to eccentric center excitation are investigated. Results show:

(1) For the rotational modes and the planet modes, the eccentric center causes some natural frequencies to increase, and the other natural frequencies to drop. For the special planet modes, the eccentric center has not effects on the natural frequencies.
(2) For the rotational modes and the planet modes, the eccentric center causes some vibrations to become weak, and the other vibrations to become strong.
(3) The eccentric center causes vibration center shift of the drive system. The eccentric center has more obvious effects on the dynamic behavior of the planets.

Acknowledgment

This project is supported by National Natural Science Foundation of China (No51075350).

References

[1] D.F. Herdeg, Electromagnetic harmonic drive low inertia servo actuator. A D 442879. Dec,1963.
[2] M. Da Lio, A. Nista and F. Viola, Electromagnetic harmonic motor with continuous control of position and torque. Proceedings of the 27^{th} Applications in the transportation industries, *Aachen* **11** (1994), 487–491.
[3] O. Barth, Harmonic piezodrive-miniaturized servo motor, *Mechatronics* **10** (2000), 545–554.
[4] X. Lizhong and Q. Lei, Displacements for an electromechanical integrated electrostatic harmonic drive, *The Journal of Strain Analysis for Engineering Design* **41**(2) (2006), 101–111.
[5] X. Lizhong and Z. Cuirong, Parametric vibration for electromechanical integrated electrostatic harmonic drive, *Mechatronics* **65**(1) (2007), 54–66.
[6] K. Ikuta, S. Makita and S. Arimoto, Non-contact magnetic gear for micro transmission mechanism. Proceedings, *IEEE Micro Electro Mechanical Systems* 1991, 125–130 Nara, Jpn.
[7] F.T. Joergensen, T.O. Andersen and P.O. Rasmussen, The cycloid permanent magnetic gear. Conference Record – IAS Annual Meeting (IEEE Industry Applications Society), v 1, Conference Record of the 2006 IEEE Industry Applications Conference – Forty-First IAS Annual Meeting, 2006, pp. 373–378.
[8] M.R. Kuehnle, Toroidgetriebe. Urkunde uber die Erteilung des deutschen Patents, 1966, 1301682.
[9] M.R. Kuehnle, H. Peeken and C. Troeder, The Toroidal drive, *Mechanical Engineering* **32**(2) (1981), 32–39.
[10] M.R. Kuehnle, Toroidal transmission and method and apparatus for making and assembling same. United States Patent, 1999, 5863273.
[11] X. Lizhong, H. Then and Y. Yulin, Contact Stresses for Toroidal drive. Journal of Mechanical Design, *Transactions of the ASME* **125**(3) (2003), 165–168.
[12] X. Lizhong and H. Xiuhong, Dynamic model of electromechanical integrated toroidal drive, *International Journal of Applied Electromagnetics and Mechanics* **22**(3–4), 199–211.
[13] X. Lizhong and F. Sunhou, Design and torque control for electromechanical integrating toroidal drive, *Mechanism and Machine Theory* **41**(2) (2006), 230–245.
[14] X. Lizhong and H. Jin, Force and stress for electromechanical integrated toroidal drive, *Structural Engineering and Mechanics* **35**(3) (2010), 383–386.